Layered Structures of Assembled Imine-Linked Macrocycles and Two-Dimensional Covalent Organic Frameworks Give Rise to Prolonged Exciton Lifetimes

Waleed Helweh, [=,†,§] Nathan C. Flanders, [=,†,§] Shiwei Wang,[†] Brian T. Phelan,[§] Pyosang Kim,[†] Michael J. Strauss,[†] Rebecca L. Li, [†] Matthew S. Kelley,[†] Matthew S. Kirschner,[†] Dillon O. Edwards, [†] Austin P. Spencer,[†] George C. Schatz,[†] Richard D. Schaller,[†,‡] William R. Dichtel,[†*] Lin X. Chen[†,§*]

[†]Department of Chemistry, Northwestern University, 2145 Sheridan Road, Evanston, IL, 60208 USA

[‡]Center for Nanoscale Materials, Argonne National Laboratory, Argonne, IL 60439, USA.

[§]Chemical Sciences and Engineering Division, Argonne National Laboratory, Argonne, IL 60439, USA.

Supplementary Information

Correspondence Address
Professor William R. Dichtel
Department of Chemistry
Northwestern University
2145 Sheridan Road
Evanston, IL 60208 (USA)
wdichtel@northwestern.edu
Professor Lin X. Chen
Department of Chemistry
Northwestern University
2145 Sheridan Road
Evanston, IL 60208 (USA)
l-chen@northwestern.edu

Table of Contents

1

Supplementary Note 1:
Femtosecond and Nanosecond TA Experimental and Analysis Details

Femtosecond transient absorption (fsTA) spectroscopy experiments were performed using a 1 kHz Ti:sapphire regeneratively-amplified laser system (Spectra-Physics MaiTai oscillator / Spitfire Pro XP amplifier) which has been described previously.[1, 2] Briefly, 0.6 mJ of the amplified laser pulses (830 nm, 100 fs, 2.8 mJ) were directed towards a 10% reflective beamsplitter where the reflected portion was used for the probe pulse and the transmitted portion was used for the pump pulse. The transmitted fundamental was reduced to a diameter of about 2 mm before driving second harmonic generation in a 2 mm thick Type I lithium triborate crystal ($\theta = 90°$, $\varphi = 28°$). The reflected fundamental and the second harmonic were both directed towards the TA spectrometer (Helios, Ultrafast Systems). The reflected fundamental was directed along an optical delay stage and then about 4 μJ were focused into a 3 mm thick sapphire window to generate a continuum ranging from 450-800 nm. The second harmonic was directed through a thin-film polarizer, set to magic angle (54.7°) with respect to the probe, and a mechanical chopper, operating at 500 Hz to block every other pulse, and attenuated to 1 μJ/pulse at the sample. The pump and probe pulses were focused to about 300 μm and 100 μm, respectively, and overlapped in the sample. The probe pulse was collimated and then focused into a fiber optic cable coupled to a CCD detector; the probe pulse and difference spectra were collected and calculated using the Helios software (Ultrafast Systems) and equation S1:

$$S(\lambda, \Delta t) = \langle -\log(I^*/I_o) \rangle \qquad \textbf{S1}$$

where $S(\lambda, \Delta t)$ is the difference signal, I^* is the intensity of a single pump-on probe-plus-signal spectra, and I_o is the intensity of a single pump-off probe spectra.

Nanosecond transient absorption (nsTA) spectroscopy experiments, described previously,[3] were performed using a 1 kHz Nd:YAG diode-pumped mode-locked laser (Ekspla PL2210) paired with a 1 kHz supercontinuum laser (Leukos STM-1-UV). An internal pulse picker reduced the Nd:YAG pulse train to 500 Hz and the fundamental was frequency-tripled internally, yielding a 500 Hz train of 355 nm (25 ps, 0.3 mJ) pulses. The third harmonic output pumped an optical parametric generator (Ekspla PG403) tuned to 415 nm, providing about 25 ps (25 μJ) laser pulses which served as the pump pulses. The supercontinuum laser was synchronized to a 1 kHz trigger from the Nd:YAG laser and output a 1 kHz train of broadband laser pulses (400 to >1600 nm, ~600 ps, 15 uJ) which were used as the probe pulse. The supercontinuum pulses were directed through a 950 nm short-pass filter to eliminate the residual 1064 nm fundamental from the supercontinuum laser. The pump pulses, attenuated to 1 uJ/pulse at the sample, and probe pulses were then focused to about 200 μm and 100 μm, respectively, and overlapped in the sample. The probe pulses were collimated and focused into an SP-2150i Acton Series spectrograph (Princeton Instruments) and recorded using a Spyder3 SG-14 (Teledyne DALSA) CCD camera. A laboratory-written application (LabVIEW 2014, National Instruments) provided the time delays to the supercontinuum laser via DG535 delay generators (Stanford Research Systems) externally triggered by the 1 kHz Nd:YAG trigger, recorded the probe pulse spectra, and calculated the difference spectra using equation S2:

$$S(\lambda, \Delta t) = -\log(\langle I^* \rangle / \langle I_o \rangle) \qquad \textbf{S2}$$

Equation S2 differs from equation S1 in that the pump-on probe-plus-signal spectra and pump-off probe spectra are first averaged before the difference spectra are calculated.

The samples for both the fs- and nsTA experiments were prepared as solutions in THF in 2 mm quartz cuvettes with an optical density of about 0.3 at 415 nm. Both the fs- and nsTA experiments were collected using a pump pulse energy of 0.2 μJ. The fsTA experiments were collected by averaging 250 difference spectra (0.5 s) at each time delay (282 total time delays ranging from -2 to 3100 ps) during a single scan of the delay stage; 6 scans of the delay stage were collected in total. The nsTA experiments were collected by averaging 1000 difference spectra (2 s) at each time delay (250 total time delays ranging from -10 to 500 ns) during a single sweep of the full set of time delays; 5 scans of the time delays were collected in total.

The fs- and nsTA spectra had the background signal, dominated by pump scatter, subtracted and were corrected for group delay dispersion in the probe pulse.

Supplementary Note 2:
DFT Calculations on Model Complexes

Ground and excited state calculations on monomer units were performed using density functional theory (DFT) and linear response time dependent density functional theory (TDDFT) with the ORCA 4.0.1 software package.[4] All calculations used the Becke exchange functional [5] with the Lee-Yang-Parr correlation functional (B3LYP),[6, 7] and the def2-TZVP basis with the def2/J auxiliary basis.[8, 9] Additionally, all calculations were performed with the RIJCOSX 'chain-of-spheres' approximation [10-12] and with TDDFT calculations using the Tamm-Dancoff approximation.[13] The geometry of the flattened configuration was approximated by performing a constrained geometry optimization restricting the dihedral angles between the rings of the monomer. Calculated absorption spectra were broadened by a single Gaussian with a width of 0.2 eV and orbitals were visualized and analyzed with the UCSF Chimera software package.[14]
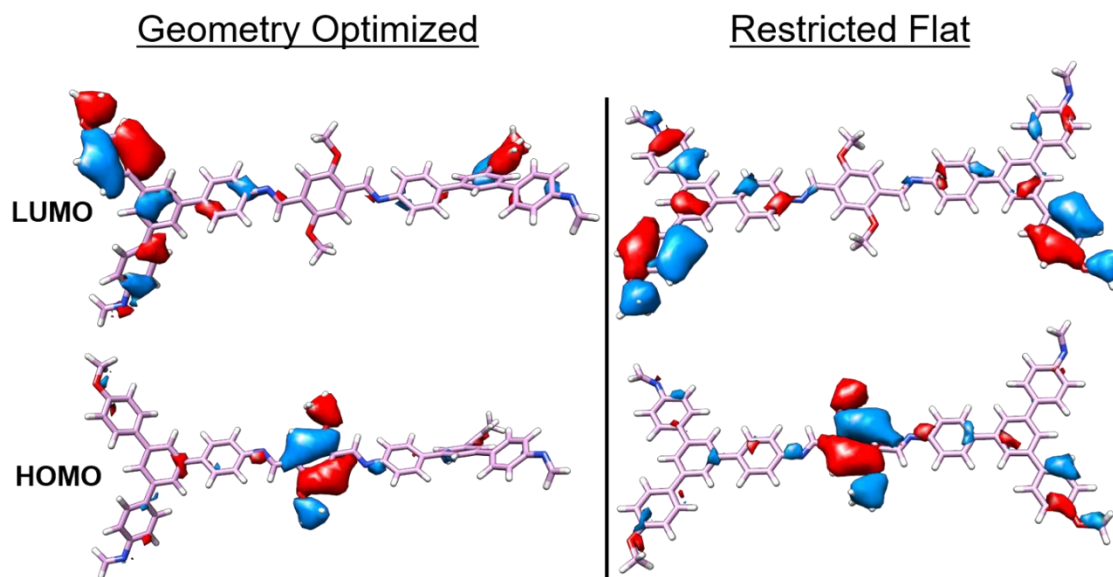
Figure S1. HOMO-LUMO diagram of a truncated model of the macrocycle, calculated by TDDFT, which includes two TAPB building blocks connected by a DiMeO-PDA building block. There are two model conformations calculated and depicted, a geometry optimized and restricted flat, reminiscent of the macrocycle and the nanotube, respectively, indicating a similar trend of the energy density migration and transition dipole.
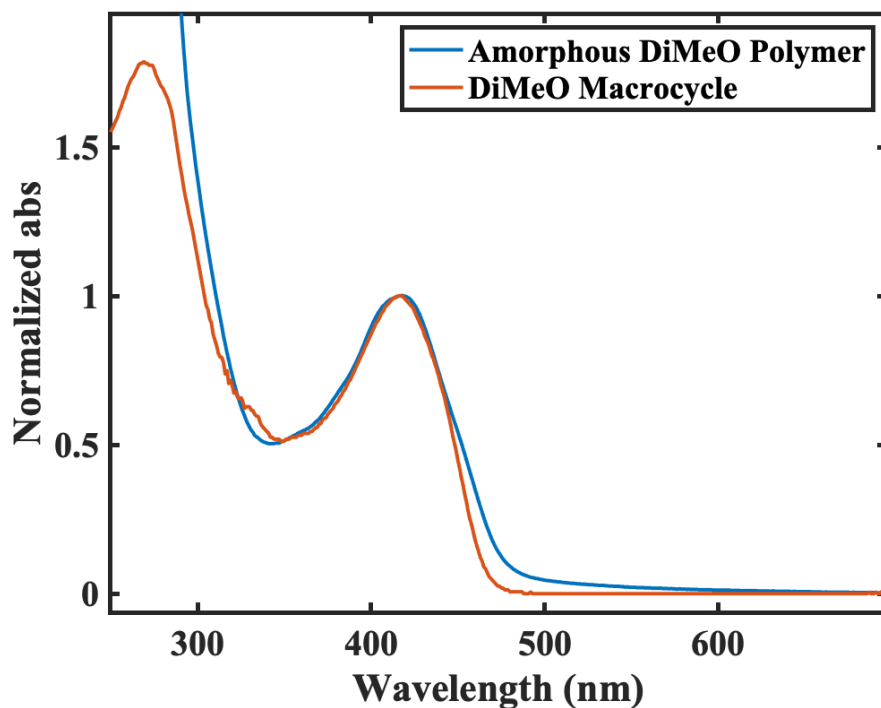

Figure S2. Comparison UV-Vis of amorphous DiMeO Polymer and DiMeO MC showing similar absorption structures.
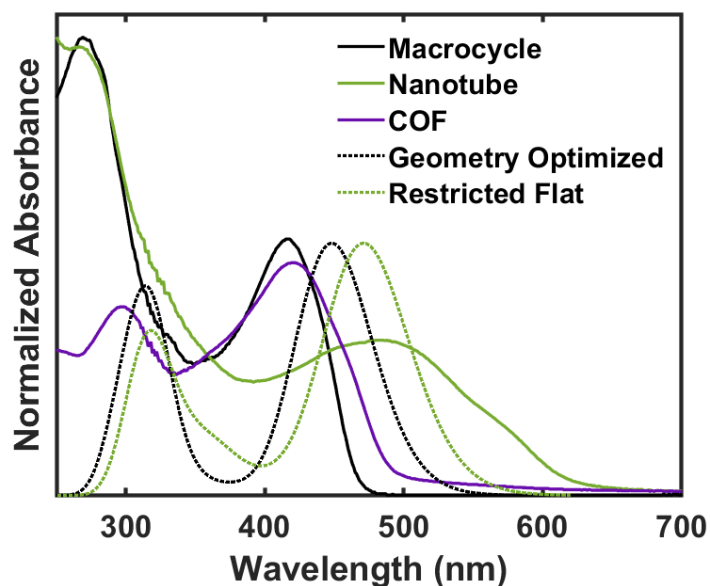
Figure S3. Comparison of the calculated absorption spectra of the two model compound conformations with the experimental absorption spectra of the macrocycle, nanotube, and covalent organic framework (COF) revealing a similar trend of a red shift of the lowest lying transition.
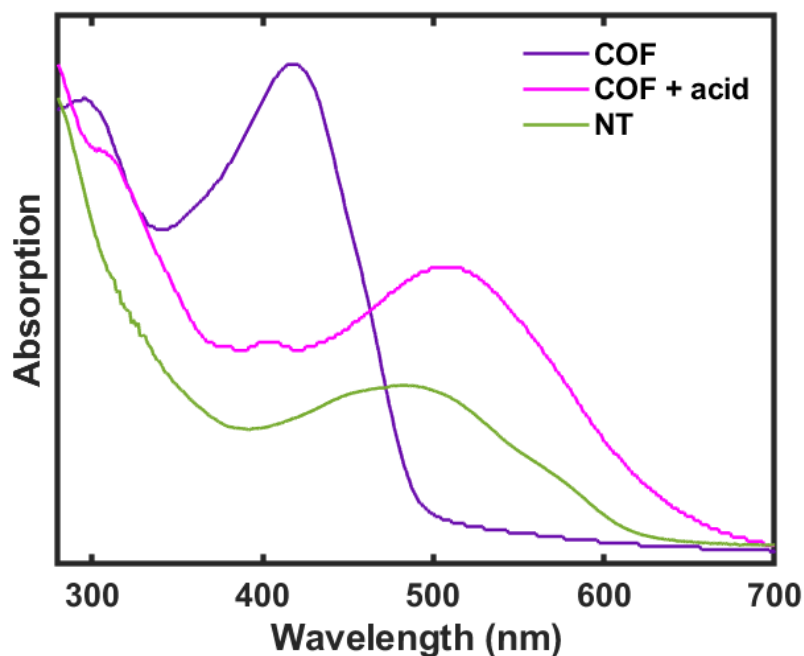
Figure S4. Steady-state absorption of the COF, NT, and COF upon protonation. Addition of large equivalents of acid to the COF protonates the imine bonds revealing a similar red-shift of the absorption as the NT.
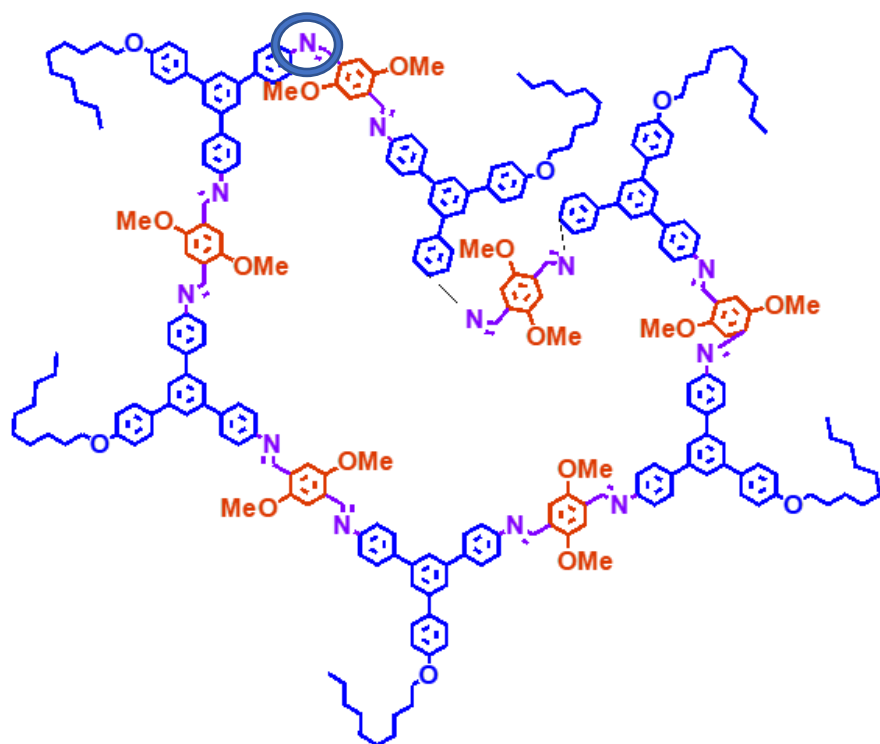
Figure S5. Strained structure with highlighted cis bond demonstrating structure is too strained to be achieved, and thus only pyramidalization is necessary for internal conversion, not trans-cis isomerism.
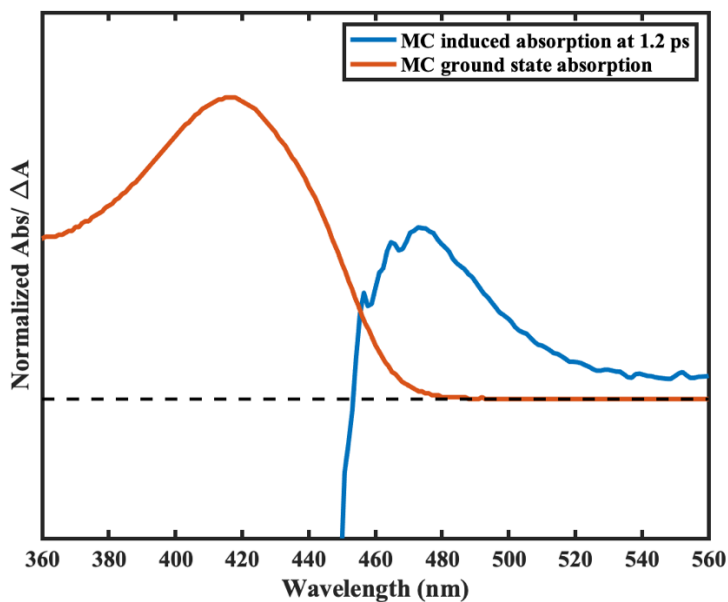
Figure S6. Ground-state (GS) absorption of MC and induced absorption following photoexcitation showing a derivative feature which indicates the induced absorption is shifted to slightly lower energy. The induced absorption likely corresponds to a vibrationally excited ground state.
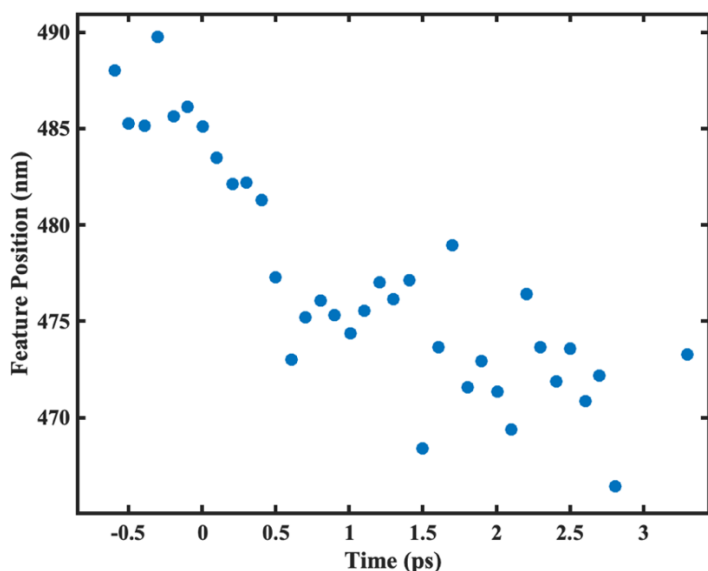
Figure S7. Wavelength position of the maximum of the blue ESA feature attributed to vibrationally excited ground state absorption of free MC revealing blue shift with time. Blue shift indicates return to original GS position.
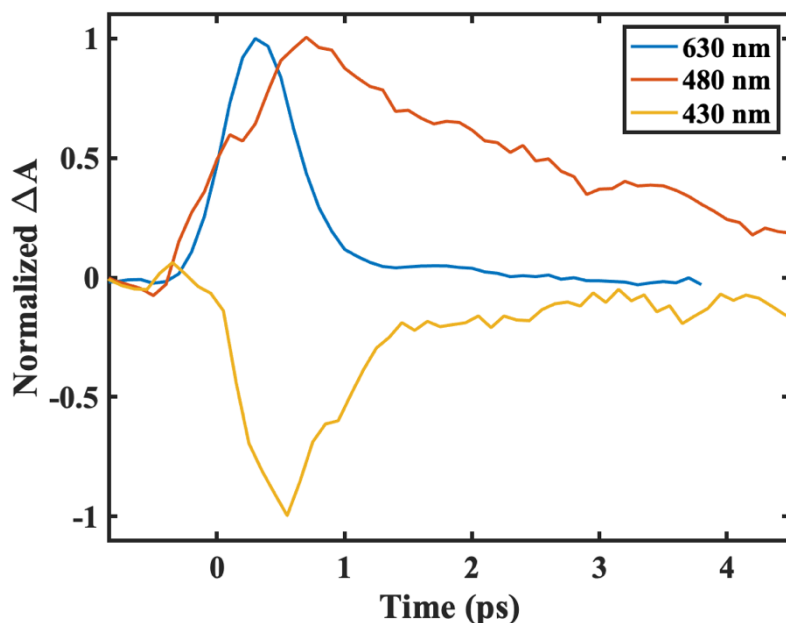

Figure S8. Comparison kinetics of amorphous DiMeO Polymer revealing divergent kinetics at different probe wavelengths. Namely, the 430 nm feature indicates ground state bleach, the redshifted 480 nm feature indicates vibrationally excited ground state absorption which recovers in 5 ps, and 630 nm indicates internal conversion of ESA feature.
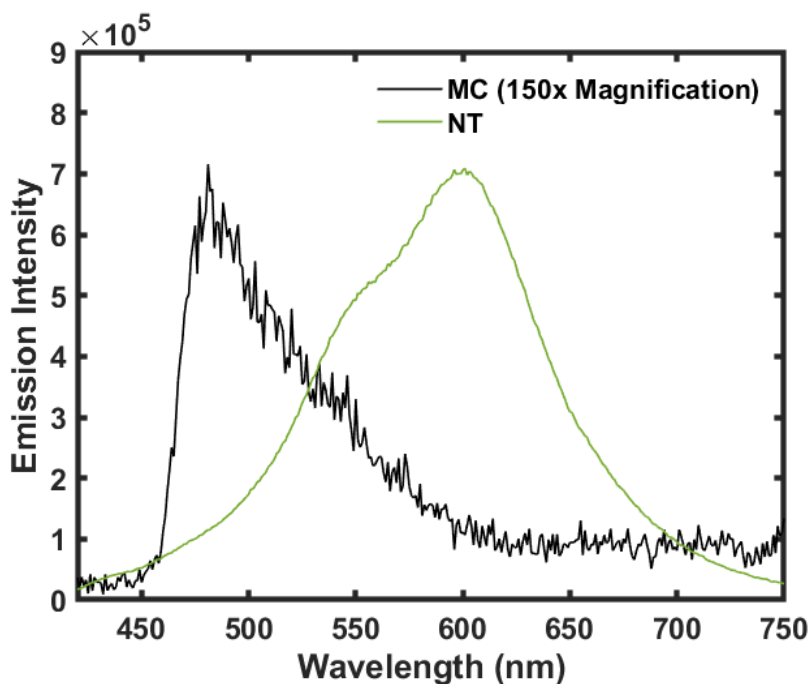
Figure S9. Steady-state fluorescence of the MC (with 150x magnification of intensity) and NT.
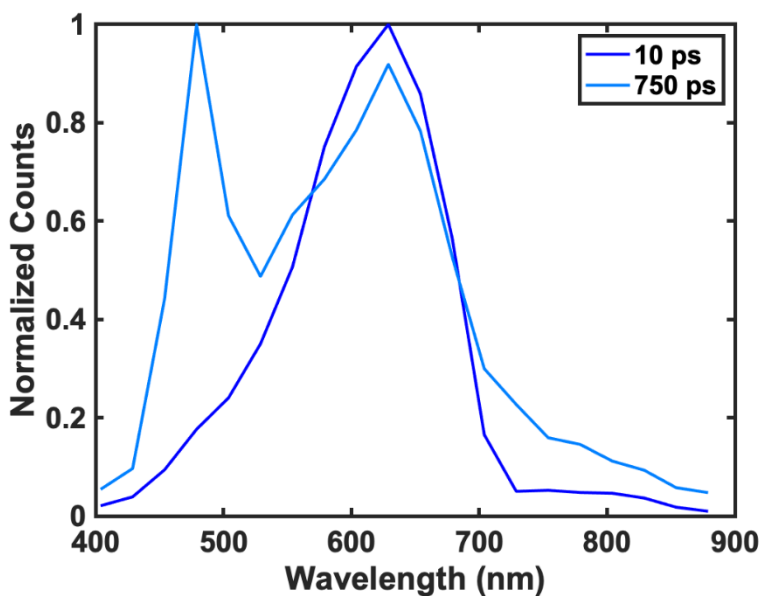

Figure S10. Spectral evolution of NT fluorescence after photoexcitation showing similar spectral features as well as evidence of offset feature present at long times (beyond 85 ps). Emission feature seen at 490 nm is pump scatter.
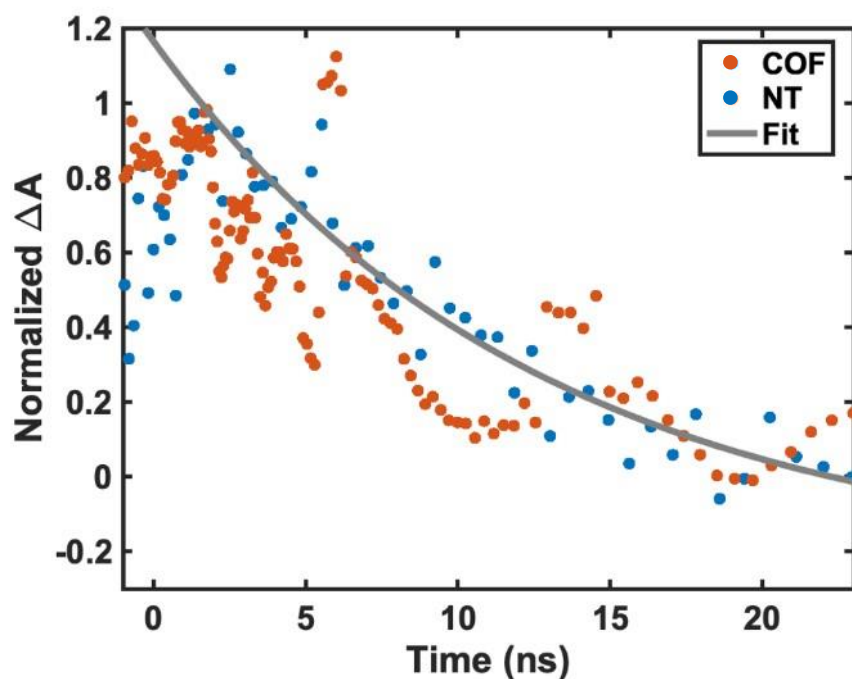
Figure S11. NSTA data of NT and COF probed at 630 nm revealing long lived kinetic decay of 12.5±2 ns. Early time decays could not be resolved on this instrument.
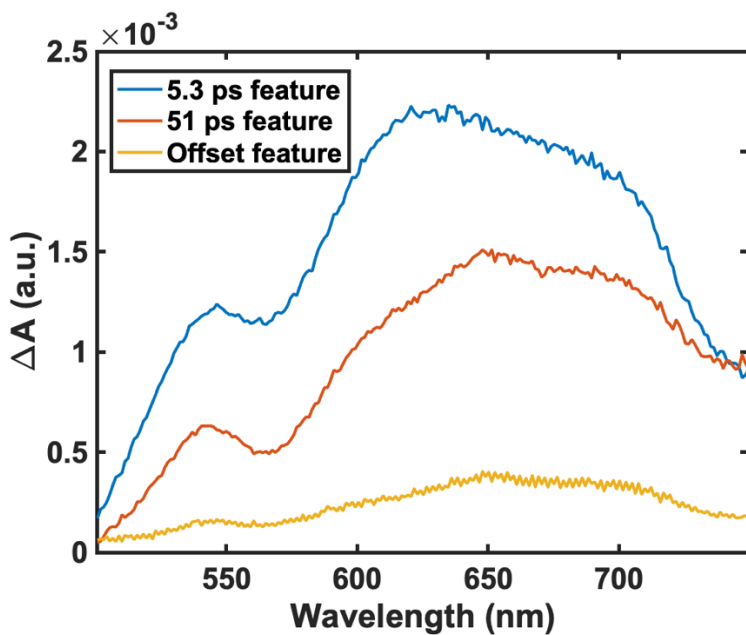

Figure S12. Results of the Global analysis of the NT revealing wavelength amplitude at respective wavelengths for both 5.3 ps component as well as 51 ps component showing similar spectral shapes.
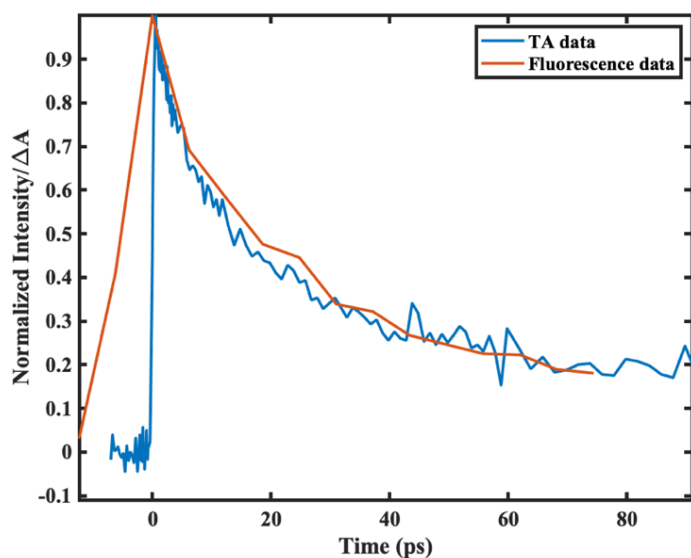
Figure S13. Time-resolved fluorescence probed at 600 nm and transient absorption signal probed at 630 nm of the NT both photoexcited at 400 nm, revealing consistent kinetics. Both decays arise from the same S1 state as inferred from the consistent kinetics.
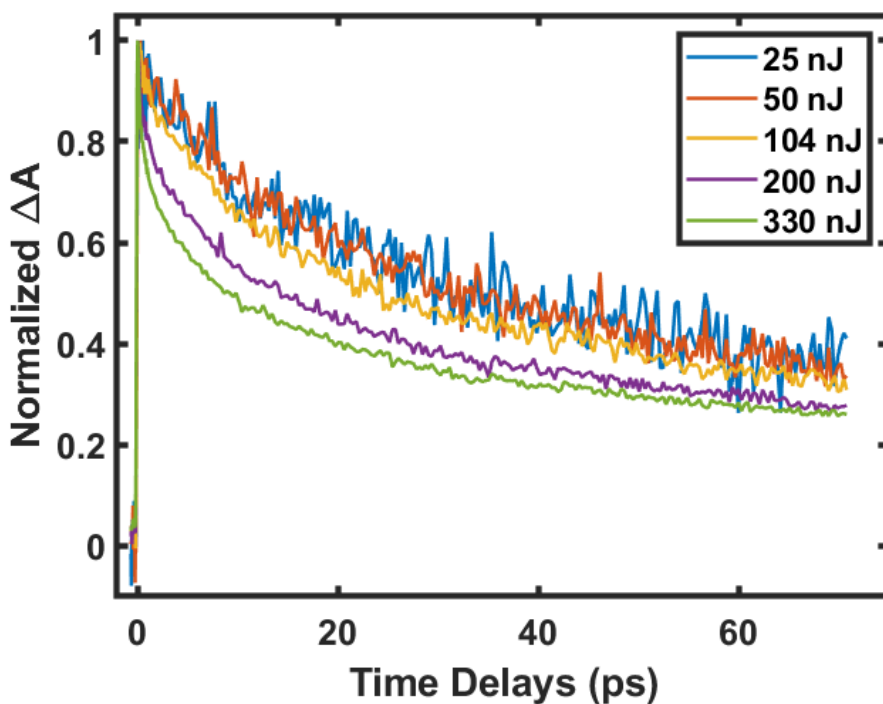

Figure S14. Power-dependent TA spectroscopy on the NT indicates the presence of multi-exciton processes at higher fluences.
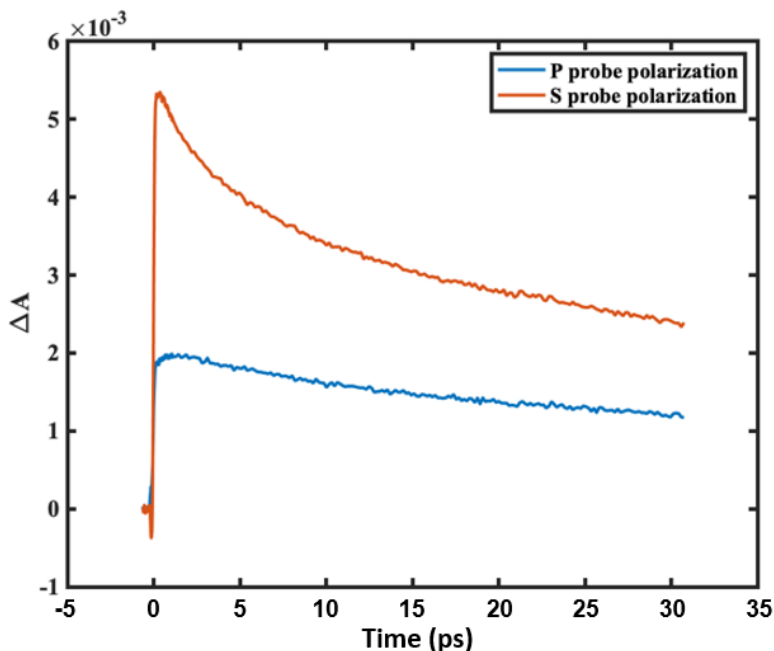
Figure S15. Transient absorption anisotropy results of NT revealing perpendicular vertical (P) and parallel Horizontal (S) probe polarization signals. P polarized probe grows in as S polarized light decays revealing depolarization through energy transfer.
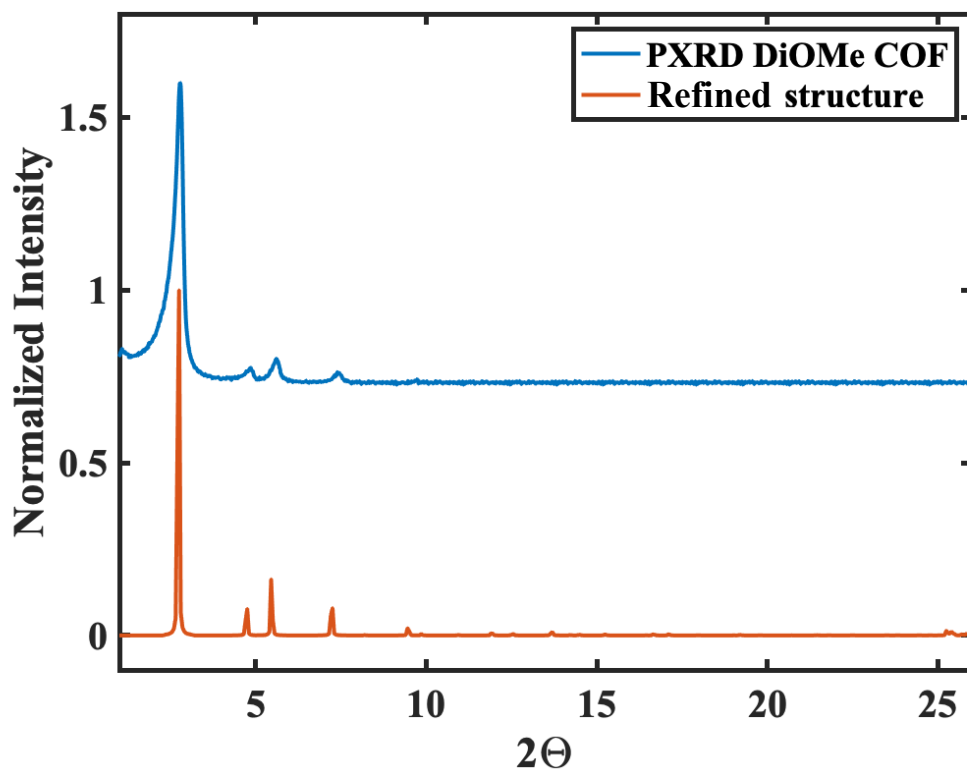

Figure S16. PXRD and Pawley refinement of TAPB-DiMeO COF for P6 structure, showing entirely eclipsed conformation is achieved upon synthesis.
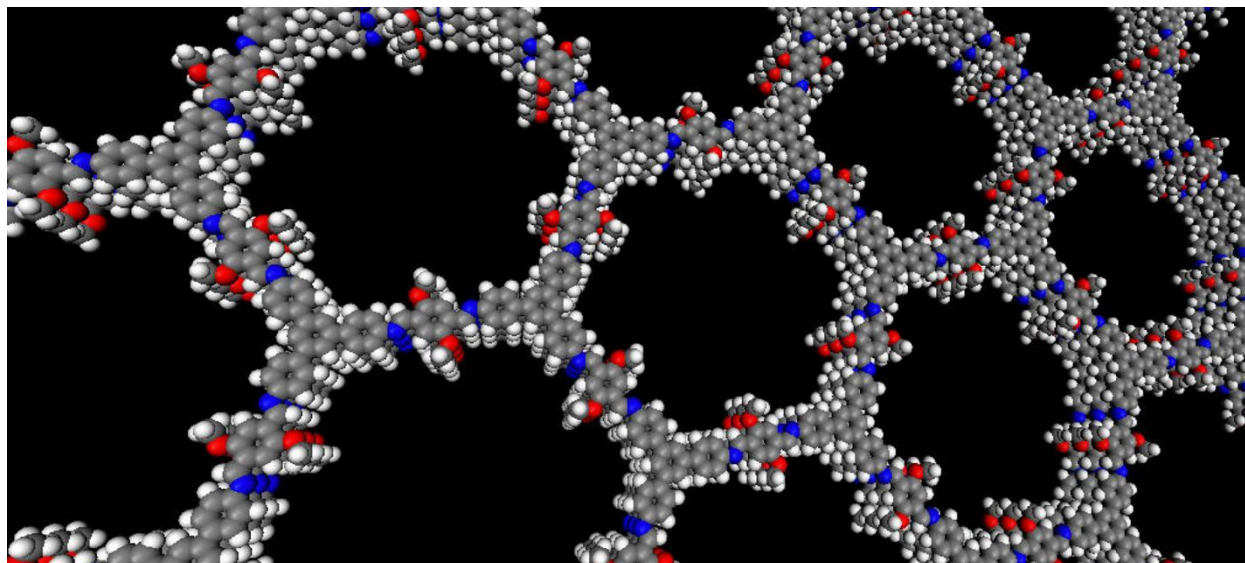
Figure S17: Resulting Structure from Pawley refinement showing 2D COF sheet eclipsed P6 structure.
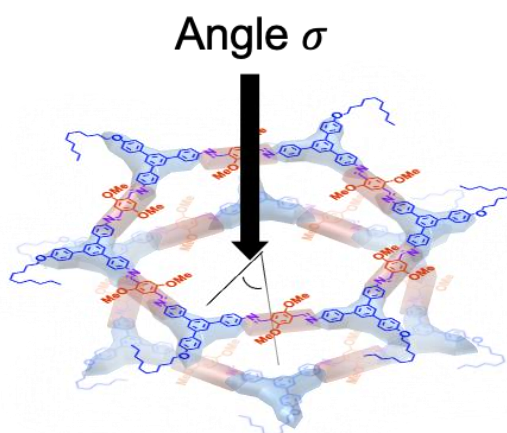

Figure S18. Schematic of the angle σ of chromophore angle relative to one another in inter-macrocycle assembly of nanotubes. The σ angle dictates the relationship between the depolarization rate and energy transfer rate.
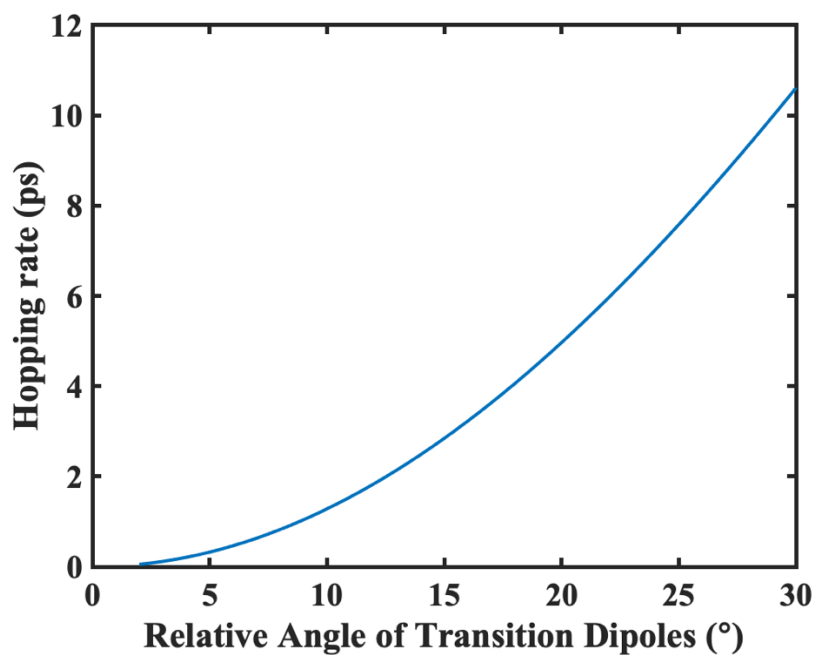
Figure S19. Relation of angle of transition dipoles, α, in the NT to the hopping rate (energy transfer rate) via the slower depolarization time component.

References:

1.	Greenfield, S. R.; Wasielewski, M. R., Near-Transform-Limited Visible and near-Ir Femtosecond Pulses from Optical Parametric Amplification Using Type-Ii Beta-Barium Borate. *Opt. Lett.* **1995,** *20* (12), 1394-1396.

2.	Hayes, D.; Kohler, L.; Hadt, R. G.; Zhang, X. Y.; Liu, C. M.; Mulfort, K. L.; Chen, L. X., Excited state electron and energy relays in supramolecular dinuclear complexes revealed by ultrafast optical and X-ray transient absorption spectroscopy. *Chem. Sci.* **2018,** *9* (4), 860-875.

3.	Hayes, D.; Kohler, L.; Hadt, R. G.; Zhang, X.; Liu, C.; Mulfort, Karen L.; Chen, L. X., Excited state electron and energy relays in supramolecular dinuclear complexes revealed by ultrafast optical and X-ray transient absorption spectroscopy. *Chemical Science* **2018,** *9* (4), 860-875.

4.	Neese, F., The ORCA program system. *Wires Comput Mol Sci* **2012,** *2* (1), 73-78.

5.	Becke, A. D., Density-Functional Thermochemistry .3. The Role of Exact Exchange. *J. Chem. Phys.* **1993,** *98* (7), 5648-5652.

6.	Lee, C. T.; Yang, W. T.; Parr, R. G., Development of the Colle-Salvetti Correlation-Energy Formula into a Functional of the Electron-Density. *Phys Rev B* **1988,** *37* (2), 785-789.

7.	Miehlich, B.; Savin, A.; Stoll, H.; Preuss, H., Results Obtained with the Correlation-Energy Density Functionals of Becke and Lee, Yang and Parr. *Chem. Phys. Lett.* **1989,** *157* (3), 200-206.

8.	Weigend, F.; Ahlrichs, R., Balanced basis sets of split valence, triple zeta valence and quadruple zeta valence quality for H to Rn: Design and assessment of accuracy. *PCCP* **2005,** *7* (18), 3297-3305.

9.	Weigend, F., Accurate Coulomb-fitting basis sets for H to Rn. *PCCP* **2006,** *8* (9), 1057-1065.

10.	Neese, F.; Wennmohs, F.; Hansen, A.; Becker, U., Efficient, approximate and parallel Hartree-Fock and hybrid DFT calculations. A 'chain-of-spheres' algorithm for the Hartree-Fock exchange. *Chem. Phys.* **2009,** *356* (1-3), 98-109.

11.	Kossmann, S.; Neese, F., Comparison of two efficient approximate Hartee-Fock approaches. *Chem. Phys. Lett.* **2009,** *481* (4-6), 240-243.

12.	Izsak, R.; Neese, F., An overlap fitted chain of spheres exchange method. *J. Chem. Phys.* **2011,** *135* (14).

13.	Hirata, S.; Head-Gordon, M., Time-dependent density functional theory within the Tamm-Dancoff approximation. *Chem. Phys. Lett.* **1999,** *314* (3-4), 291-299.

14.	Pettersen, E. F.; Goddard, T. D.; Huang, C. C.; Couch, G. S.; Greenblatt, D. M.; Meng, E. C.; Ferrin, T. E., UCSF chimera - A visualization system for exploratory research and analysis. *J. Comput. Chem.* **2004,** *25* (13), 1605-1612.